JOURNAL OF GEOPHYSICAL RESEARCH, VOL. 97, NO. D18, PAGES 20,455–20,468, DECEMBER 20, 1992

A Bidirectional Reflectance Model of the Earth's Surface for the Correction of Remote Sensing Data

JEAN-LOUIS ROUJEAN[1]

Laboratoire d'Etudes et Recherches en Télédétection Spatiale, Toulouse Cedex, France

MARC LEROY

Centre National d'Etudes Spatiales, Toulouse Cedex, France

PIERRE-YVES DESCHAMPS

Laboratoire d'Optique Atmosphérique, Université des Sciences et Techniques de Lille, Villeneuve d'Asq, France

A surface bidirectional reflectance model has been developed for the correction of surface bidirectional effects in time series of satellite observations, where both sun and viewing angles are varying. The model follows a semiempirical approach and is designed to be applicable to heterogeneous surfaces. It contains only three adjustable parameters describing the surface and can potentially be included in an algorithm of processing and correction of a time series of remote sensing data. The model considers that the observed surface bidirectional reflectance is the sum of two main processes operating at a local scale: (1) a diffuse reflection component taking into account the geometrical structure of opaque reflectors on the surface, and shadowing effects, and (2) a volume scattering contribution by a collection of dispersed facets which simulates the volume scattering properties of canopies and bare soils. Detailed comparisons between the model and in situ observations show satisfactory agreement for most investigated surface types in the visible and near-infrared spectral bands. The model appears therefore as a good candidate to reduce substantially the undesirable fluctuations related to surface bidirectional effects in remotely sensed multitemporal data sets.

1. INTRODUCTION

Applications of remote sensing of solar radiation reflected by the Earth-atmosphere system to observe the evolution of Earth's resources have become increasingly important. When a high frequency of observations is required, the land resources may be monitored using wide field of view sensors such as the advanced very high resolution radiometer (AVHRR) from NOAA or pointable sensors such as System Probatoire d'Observation de la Terre (SPOT), with large variations of the viewing configuration. Another possibility is to use geostationary sensors such as Meteosat, often with large variations of solar illumination conditions. A given point on Earth is then observed in time series of sensor data characterized by a large range of view or sun angles.

The surface reflectance bidirectional effects can in many circumstances add a significant component of noiselike fluctuations to the time series [*Taylor and Stowe*, 1984; *Gutman*, 1987; *Roujean et al.*, 1992]. The magnitude of these effects can lead to large errors, in particular when observing the phenological evolution of vegetation on a regional scale [*Gutman*, 1987; *Roujean et al.*, 1992]. A model of correction of the surface reflectance bidirectionality is thus necessary to normalize the sensor data.

A model of correction of bidirectional effects is also needed in other remote sensing applications. The estimation of the directional and diffuse albedos from a sample of bidirectional reflectance observations requests the assessment of such a model. Also, surface anisotropy algorithms can serve as lower boundary conditions for atmosphere radiative transfer models.

Parallel to the necessary development of in situ measurements of bidirectional reflectance distribution functions [e.g., *Kriebel*, 1978; *Kimes*, 1983; *Kimes et al.*, 1985; *Deering and Leone*, 1986], considerable attention has been given in recent years to the elaboration of analytical and nonanalytical models of these effects (see the review by *Goel* [1988]). We restrict the discussion here to analytical models, which are the only models of relevance for the sensor data correction problem. Some of them are based on the analysis of the geometrical structure of reflectors at the surface [e.g., *Egbert*, 1976, 1977; *Otterman*, 1981; *Otterman and Weiss*, 1984; *Deering et al.*, 1990]. A number of other models have considered the bare ground [*Hapke*, 1963, 1981, 1986; *Lumme and Bowell*, 1981; *Norman et al.*, 1985] or the canopy [e.g., *Suits*, 1972; *Ross*, 1981; *Verhoef*, 1984, 1985; *Camillo*, 1987; *Verstraete et al.*, 1990] as a turbid medium made of scattering and absorbing particles with given geometrical and optical properties and have proposed analytical solutions of the radiative transfer equation with various degrees of complexity.

All these models are, however, devoted to the examination of thematically homogeneous surfaces, whereas a pixel of a satellite sensor, whose size ranges from tens of meters to a few kilometers, contains generally a heterogeneous mixture of bare soils and vegetation canopies. Moreover, the

[1]Now at Centre National de Recherches Météorologiques, Toulouse, France.

Paper number 92JD01411.
0148-0227/92/92JD-01411$05.00

number of surface parameters of these models, generally greater than or equal to 5, turns out to be too high in practice for the correction of sensor data. For example, few AVHRR data can be obtained usually within a period comparable to the vegetation evolution time scale, about 10 days, principally because of cloud contamination. This number of sensor data is generally too small to statistically adjust a large number of parameters. The empirical models of *Minnaert* [1941], *Walthall et al.* [1985], and *Shibayama and Wiegand* [1985] contain 2, 3, and 4 parameters, respectively; however, their empirical nature makes them difficult to apply to a wide variety of targets. Moreover, the first of these models does not contain any dependence upon the relative azimuth between the sun and viewing direction, which is a major shortcoming, and the two latter models do not satisfy the reciprocity conditions, by which the bidirectional reflectance should remain invariant by inverting the sun and view directions.

The present paper describes a semiempirical model of surface reflectance bidirectional effects, which intends to overcome the above mentioned difficulties. The model contains three parameters, a number sufficiently small to normalize a time series of sensor data in a relatively small period of observation. Simple physical representations of the surface are used as a guide to obtain the functional dependence of the surface reflectance upon the sun and view angles. A series of assumptions is then made to reduce the number of surface parameters to three, and to linearize the model as a function of its surface parameters to make it easily applicable to heterogeneous surfaces.

The model is developed in section 2 and is compared in detail in section 3 with a series of in situ measurements of bidirectional reflectance over a wide variety of surface types. Section 4 discusses the possibilities of application of the model to the normalization of time series of sensor data.

2. BIDIRECTIONAL REFLECTANCE MODEL

2.1. *General Considerations*

The concepts of our model have been guided by the examination of the comprehensive set of observational data and associated physical pictures which have been published in the literature [e.g., *Hapke and van Horn*, 1963; *Coulson*, 1966; *Coulson and Reynolds*, 1971; *Kriebel*, 1978; *Eaton and Dirmhirn*, 1979; *Kimes*, 1983; *Kimes et al.*, 1985, 1986; *Deering and Eck*, 1987]. According to these works, the observed bidirectional diagrams show specific and repetitive signatures. One important signature of many bare soils and canopies is to have strong backscattering characteristics. This is interpreted as an effect of the geometrical structure of reflectors on the surface [*Egbert*, 1977; *Kimes*, 1983]; as the sensor direction moves away from the solar direction, the reflectance decreases, since two phenomena occur in the sensor's field of view. First, the relative proportion of shadowed surfaces increases, and second, the proportion of viewed facets with normals that deviate from the solar direction increases, causing decreased solar irradiance on these facets. Another important signature, occurring in particular for dense canopies, is at all sun angles and spectral bands a minimum reflectance near nadir viewing, and increasing reflectance with increasing off-nadir view angle for all view azimuth directions. (The hot spot phenomenon, mentioned later in the text, is an exception to this general behavior.) This is thought to be caused by the shading of lower canopy layers by components in the upper layers and by viewing different proportions of the layer components as the sensor view angle changes [*Kriebel*, 1978; *Kimes*, 1983]. Clearly, volume effects are at the origin of this latter phenomenon.

The surface reflectance may then be viewed as a combination of two different components representative of these two different bidirectional signatures.

1. First is a component of diffuse reflection by material surfaces, of reflectance ρ_{geom}, which takes into account the geometrical structure of opaque reflectors and shadowing effects. This component is modeled here by vertical opaque protrusions reflecting according to Lambert's law, placed on a flat horizontal plane. They represent mainly irregularities and roughness of bare soil surfaces but may also represent structured features of low transmittance canopies. This modeling has been adopted for its capability to describe simply the shadowing effects.
2. Second is a component of volume scattering, of reflectance ρ_{vol}, where the medium is modeled as a collection of randomly located facets absorbing and scattering radiation. The facets represent mainly leaves of canopies, characterized by a nonnegligible transmittance, but can also model the behavior of dust, fine structures, and porosity of bare soils. A simple radiative transfer model is used to describe this component.

A discussion of the involved length scales seems appropriate at this stage. We can identify two observational length scales, which are the sensor pixel scale, from tens of meters to a few kilometers, and the ground radiometer length scale, from about one meter to a few meters, hereafter referred to as the subpixel scale or subpixel surface. Within the sensor pixel scale, the Earth's surface is frequently highly heterogeneous, while the surface is generally thematically homogeneous at the subpixel scale. However, even "homogeneous" surfaces at the subpixel scale are in fact highly heterogenous at smaller scales, with the presence of stalks, leaves, ears, buds, etc., and soil roughness at various scales. The geometrical and volume components identified above may operate at various length scales. Opaque structured features with associated shadows exist at relative large scales (shadows of trees, stalks, stones). They also exist on microscales (larger than a few microns) associated with soil or leaf roughness [*Irvine*, 1966]. The facets of the volume component have a dimension which ranges from the size of leaves of a canopy (a few centimeters) down to the size of microdust in bare soils (a few microns).

2.2. *Estimate of the Geometric Scattering Component* ρ_{geom}

The geometric scattering component is evaluated by assuming that the subpixel surface contains a large number of identical protrusions (Figure 1), the average horizontal surface associated with each protrusion being S. Each protrusion is modeled by a vertical wall of height h, width b, and length l much larger than b and h (see the appendix). The long-wall protrusion shape has been chosen for convenience to permit an easy analytical reduction of the equations. The exact protrusion shape should not be of importance anyway, since the macroscopic bidirectional behavior of the pattern has been found by *Egbert* [1977] to be rather insensitive to the adopted protrusion shape. Each illuminated surface of the protrusion and of the background is assumed Lambertian

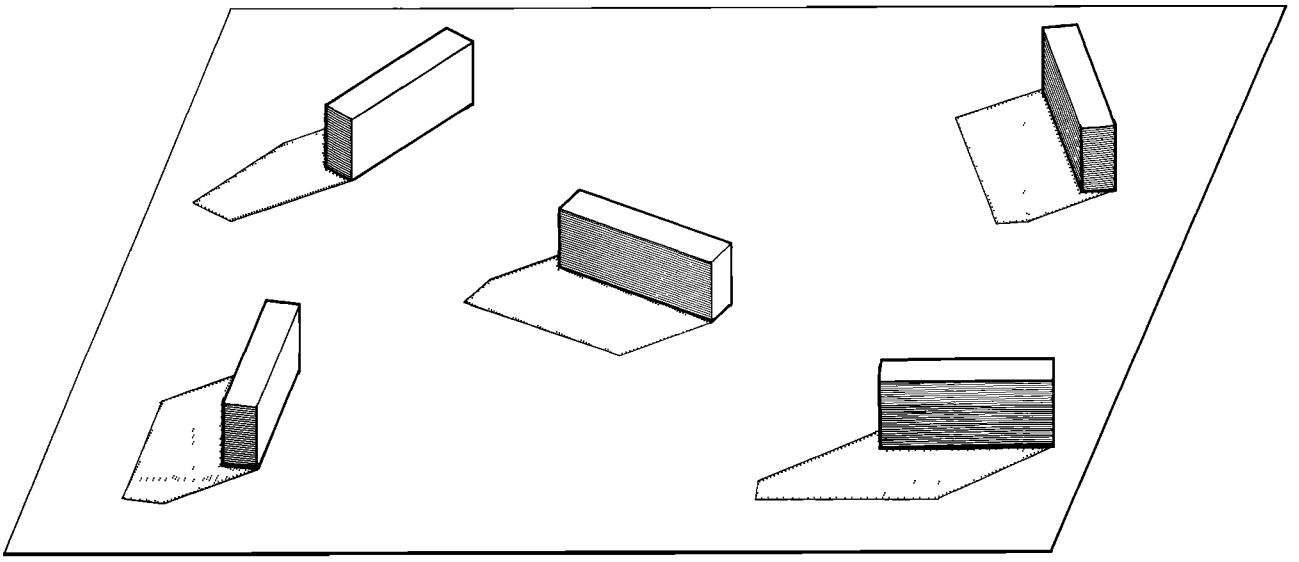

Fig. 1. Random distribution of protrusions inside a subpixel surface.

of reflectance ρ_0, while the shadowed areas are taken absolutely dark. The orientations of the walls within the subpixel surface are taken at random. The spacing between protrusions, and the solar and viewing angle ranges, are assumed such that mutual shadowing between protrusions can be neglected.

The calculation of the bidirectional reflectance associated with this system is derived with no further assumption in the appendix. The result is

$$\rho_{\text{geom}} = \rho_0\left[1 + \frac{hl}{S} f_1(\theta_s, \theta_v, \phi)\right] \tag{1}$$

where

$$f_1(\theta_s, \theta_v, \phi) = \frac{1}{2\pi}[(\pi - \phi)\cos\phi + \sin\phi]tg\theta_s tg\theta_v$$

$$-\frac{1}{\pi}(tg\theta_s + tg\theta_v + \sqrt{tg\theta_s^2 + tg\theta_v^2 - 2tg\theta_s tg\theta_v \cos\phi}) \tag{2}$$

In these expressions, θ_s and θ_v are the sun and view zenith angles, respectively, and ϕ is the relative azimuth between sun and sensor directions, chosen by convention to be between zero and π.

The function f_1, displayed in Figure 2 (top), depends only on sun and view angles, and appears as the difference of two positive terms. The first term corresponds to slope effects where the changing orientation of the vertical wall relative to the sun causes changing irradiance on these vertical surfaces. This term is basically similar to that found by *Suits* [1972] or *Otterman* [1981] in similar protrusion analysis (vertical facets with random azimuthal orientation). The second term corresponds to the account of shadowed and unviewed areas and is to our knowledge original.

The analysis of the variations of f_1 as a function of θ_v in the principal plane shows that f_1 presents a local maximum in the backscattering direction for $\theta_v = \theta_s$, $\phi = 0°$, only when the sun zenith angle θ_s is below a limit given by θ_s = arc $tg(4/\pi) \approx 51°$. When θ_s goes beyond this limit, f_1 increases monotonically with θ_v. The function f_1 is strongly dependent on the azimuth, with an enhancement in the backscattering direction and a depletion in the forward-scattering direction, and vanishes for observations at nadir with a sun at zenith. Note that the divergent behavior of f_1 when θ_v approaches $\pi/2$ originates from the fact that we have neglected mutual shadowing between protrusions. Such extreme viewing geometries are, however, far from being reached by usual satellite observations.

2.3. *Estimate of Scattering by the Volume Component* ρ_{vol}

For the estimation of the volume scattering component, we consider a homogeneous medium made of randomly located scattering plane facets of volume density N. This medium is placed above a reference flat horizontal surface of Lambertian reflectance ρ_0 (Figure 3). Each facet is characterized by an area σ, a Lambertian reflectance r, and an isotropic transmittance t. The medium has a height $z_{\max}$ above the reference surface, corresponding to a facet area index $F = N\sigma z_{\max}$. When the medium is made of leaves, F stands for the leaf area index (LAI) of the canopy [*Ross*, 1981].

The radiative transfer in the medium is solved simply by assuming the single scattering approximation, that is, the upward emergent radiation on top of the medium is made of photons which have been scattered only once on a given facet or on the reference surface, without encountering other facets in their incident and reflected optical paths. The expression of the bidirectional reflectance with these assumptions reads

$$\rho_{\text{vol}} = \frac{w}{4N\sigma}\frac{P(\theta_s, \theta_v, \phi)}{\cos\theta_s \cos\theta_v} \cdot \frac{1 - \exp\{-F[(G(\theta_s)/\cos\theta_s) + (G(\theta_v)/\cos\theta_v)]\}}{[G(\theta_s)/\cos\theta_s] + [G(\theta_v)/\cos\theta_v]} + \rho_0 \exp\left[-F\left(\frac{G(\theta_s)}{\cos\theta_s} + \frac{G(\theta_v)}{\cos\theta_v}\right)\right] \tag{3}$$

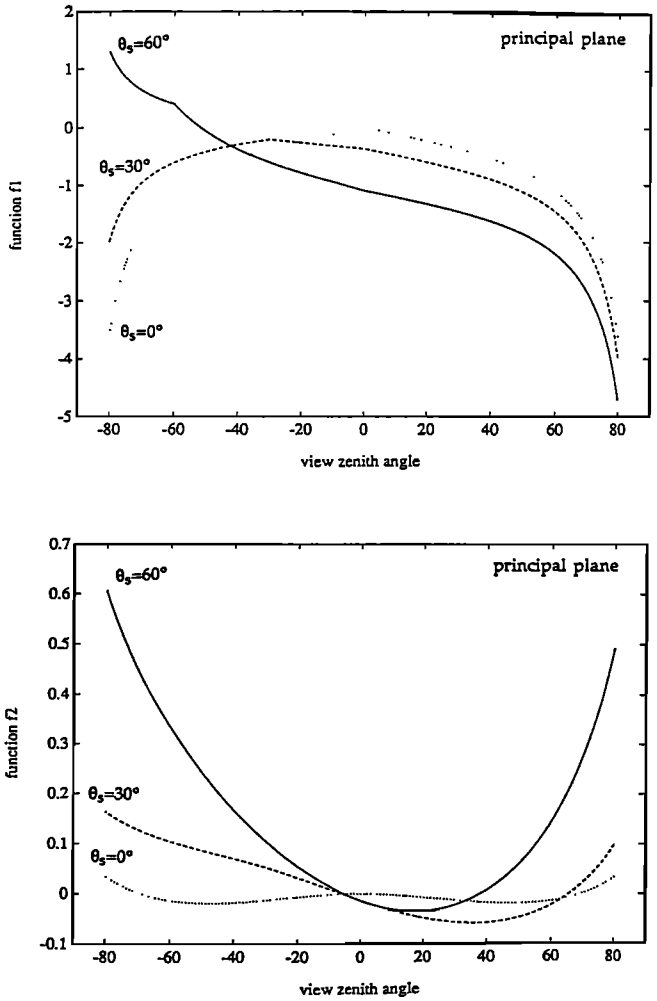

Fig. 2. Diagrams showing the functions f_1 and f_2 (equations (2) and (8)) for three sun angles θ_s, as a function of θ_v, in the principal plane. Positive (negative) θ_v correspond to forward (backward) scattering.

where w is the volume scattering coefficient, $G(\theta)$ is the so-called facets area orientation function for a radiant beam oriented at θ [*Ross*, 1981], and $P(\theta_s, \theta_v, \phi)$ is the phase function of the medium. In (3) the distribution function of the facets has been taken independent of ϕ. If we assume moreover that this distribution function is isotropic (the orientation of the facets' normals is taken at random), then the quantities w, G, and P have the following simple expressions [*Ross*, 1981]:

$$G(\theta_s) = G(\theta_v) = \frac{1}{2} \tag{4}$$

$$w = N\sigma \frac{r + t}{2} \tag{5}$$

$$P(\theta_s, \theta_v, \phi) = \frac{8}{3\pi} \frac{[(\pi - \xi)\cos\xi + \sin\xi]r + (-\xi\cos\xi + \sin\xi)t}{r + t} \tag{6}$$

where ξ is the phase or scattering angle (Figure 3), related to conventional angles by

$$\cos\xi = \cos\theta_s \cos\theta_v + \sin\theta_s \sin\theta_v \cos\phi$$

The single scattering approximation is valid when the absorption coefficient of the facets is high, which is the case of leaves in the visible spectral band, and probably of most dust particles of bare soils. This approximation is not valid, however, for leaves in the near-infrared spectral band characterized by a relatively low absorption. But it has been shown that the additional interactions due to successive scattering orders have a bidirectional signature whose amplitude decreases sharply as the scattering order increases [*Rondeaux*, 1990]. Thus, in a first approximation, the multiple scattering interactions tend to add to the single scattering radiant field a significant but roughly isotropic contribution [*Rondeaux*, 1990]. As a result, the modeling of bidirectional effects proposed in (3)–(6) remains approximately valid, the isotropic contribution resulting from multiple scattering being included in the Lambertian term ρ_0.

We make at this point two further approximations.

1. Considering that the model must be a linear function of its surface parameters to be able to extend the model to the heterogeneous surface situation, we choose to approximate the function

$$f(\theta_s, \theta_v) = \left\{1 - \exp\left[-\frac{F}{2}\left(\frac{1}{\cos\theta_s} + \frac{1}{\cos\theta_v}\right)\right]\right\} \cdot (\cos\theta_s + \cos\theta_v)^{-1}$$

appearing in (3) by the simpler function

$$\frac{1 - e^{-bF}}{\cos\theta_s + \cos\theta_v},$$

where b is a constant which represents a rough average of (1/2)/(cos θ_s + cos θ_v) for realistic variations of θ_s and θ_v. (A typical value of b is 1.5 for a range of θ_v and θ_s between 0° and 60°; the exact value has no incidence on the angular functions of the reflectance.) The above approximation is

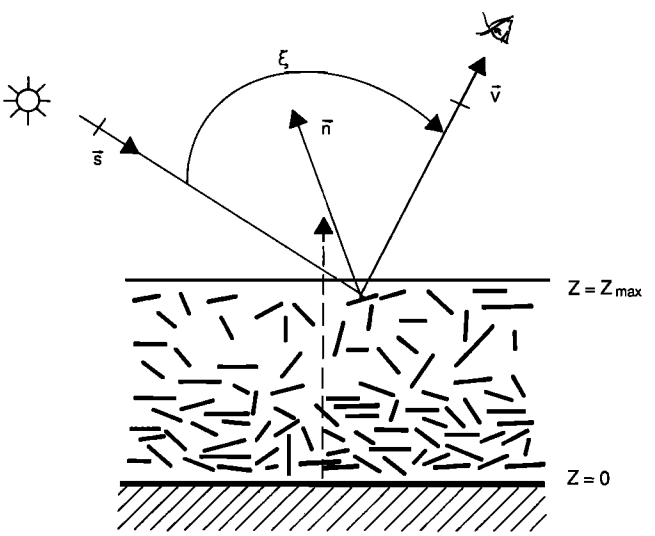

Fig. 3. Single scattering on an infinite discrete medium made of randomly distributed facets.

certainly good for optically thick media ($F \gg 1$), where the exponential term may be neglected in front of 1, and for F close to zero, where both approximate and exact functions vanish. This approximation is rather gross for $F \leq 1$, with induced relative errors which can reach 50% in the most unfavorable configurations, when both θ_v and θ_s are small. A better approximation in that case would be to take the optically thin approximation $f(\theta_s, \theta_v) = (F/2)/\cos\theta_s \cos\theta_v$, whereas our simpler function reduces when $F \ll 1$ to $bF/(\cos\theta_s + \cos\theta_v)$. The two latter functions both increase monotonically with θ_s and θ_v, but are somewhat different. However, numerical tests using these two functions alternatively against the observational measurements described in section 3, have led to quite comparable correlation results. Note also that it has seemed to us preferable to describe more accurately the optically thick domain rather than the optically thin one, since the relative contribution of the volume component to the total reflectance is expected to be weaker in the optically thin case.

2. Second, in an attempt to reduce the number of free parameters, we take $r = t$, an assumption which appears reasonable for leaves both in the visible and near-infrared regions, but may become questionable for dust particles of bare soils.

Then (3)–(6) may be rewritten

$$\rho_{\text{vol}} = r\left[\tfrac{1}{3} + f_2(\theta_s, \theta_v, \phi)\right](1 - e^{-bF}) + \rho_0 e^{-bF} \quad (7)$$

where

$$f_2(\theta_s, \theta_v, \phi) = \frac{4}{3\pi}\frac{1}{\cos\theta_s + \cos\theta_v} \cdot \left[\left(\frac{\pi}{2} - \xi\right)\cos\xi + \sin\xi\right] - \frac{1}{3} \quad (8)$$

The function f_2 has been defined such that it cancels for $\theta_v = \theta_s = 0°$, as does f_1. This function, contrary to f_1, has relatively little dependence on azimuth ϕ, especially at high sun zenith angles θ_s. Figure 2 (bottom) shows that f_2 has a minimum in the principal plane, on the forward-scattering side. The function f_2 increases with θ_v, at least when θ_v is sufficiently large, for all azimuths ϕ.

2.4. *Complete Model Expression*

The final step for the completion of our model is to combine the geometric and volume components described in sections 2.2 and 2.3. This combination is made in an empirical way, by assuming that the bidirectional reflectance $\rho(\theta_s, \theta_v, \phi)$ of the considered subpixel scale surface can be expressed as

$$\rho(\theta_s, \theta_v, \phi) = \alpha\rho_{\text{geom}} + (1 - \alpha)\rho_{\text{vol}} \quad (9)$$

where α is an empirical coefficient which characterizes the relative weight of the geometric and volume component in the final bidirectional signature. Equation (9) assumes that a partition of the subpixel surface exists, with a fraction α of the subpixel surface dominated by geometric effects, while a fraction $(1 - \alpha)$ is dominated by volume effects.

From (1), (7), and (9), our bidirectional reflectance model may be written

$$\rho(\theta_s, \theta_v, \phi) = k_0 + k_1 f_1(\theta_s, \theta_v, \phi) + k_2 f_2(\theta_s, \theta_v, \phi) \quad (10)$$

where

$$k_0 = \rho_0[\alpha + (1 - \alpha)e^{-bF}] + \frac{r}{3}(1 - e^{-bF})(1 - \alpha) \quad (11)$$

$$k_1 = \frac{hl}{S}\rho_0\alpha \quad (12)$$

$$k_2 = r(1 - e^{-bF})(1 - \alpha) \quad (13)$$

and f_1 and f_2 are simple analytic functions of the solar and viewing geometric angles, (2) and (8). The parameters k_0, k_1, and k_2 are related to our model parameters of the subpixel-scale surface, the background and protrusion reflectance ρ_0, the average height h and length l of surface protrusions, the horizontal surface S associated with each protrusion, the facet reflectance r and the facet area index F (LAI in the case of a canopy). The parameter k_0 represents the bidirectional reflectance for $\theta_s = \theta_v = 0$. Note that the model of (10) is reciprocal (as it should), that is, it remains invariant by exchanging the variables θ_s and θ_v and keeping invariant the variable ϕ.

2.5. *Properties of the Model and Discussion*

The linearity of (10) with respect to the surface parameters induces the possibility of generalizing this equation, from a thematically homogeneous subpixel surface to an heterogeneous surface of a sensor pixel. Assume, for example, that the surface S_0 of a sensor pixel is made of a large number of homogeneous surfaces S_i, characterized by their surface parameters k_{0i}, k_{1i}, and k_{2i}. The apparent bidirectional reflectance seen by the sensor for this pixel still assumes the form of (10), where the global parameters k_0, k_1, k_2 of the heterogeneous surface are related to the local surface parameters by equations such as

$$k_0 = \frac{1}{S}\sum_i k_{0i}S_i \qquad k_1 = \frac{1}{S}\sum_i k_{1i}S_i \qquad k_2 = \frac{1}{S}\sum_i k_{2i}S_i$$

The model also provides a way to relate the directional albedo (the fraction of the radiation flux incident at θ_s, reflected by the surface):

$$a(\theta_s) = \frac{2}{\pi}\int_0^{\pi} d\phi \int_0^{\pi/2} \rho(\theta_s, \theta_v, \phi)\cos\theta_v \sin\theta_v \, d\theta_v \quad (14)$$

to the above-mentioned surface parameters.

When carrying out the integral of (14) with the expression of (10) for $\rho(\theta_s, \theta_v, \phi)$, the following predictive relation is found:

$$a(\theta_s) = k_0 + k_1 I_1 + k_2 I_2 \quad (15)$$

where

$$I_1 = -0.9946 - 0.0281 \times tg\theta_s - 0.0916 \times tg^2\theta_s + 0.0108 \times tg^3\theta_s$$

$$I_2 = -0.0137 + 0.0370 \times tg\theta_s + 0.0310 \times tg^2\theta_s - 0.0059 \times tg^3\theta_s.$$

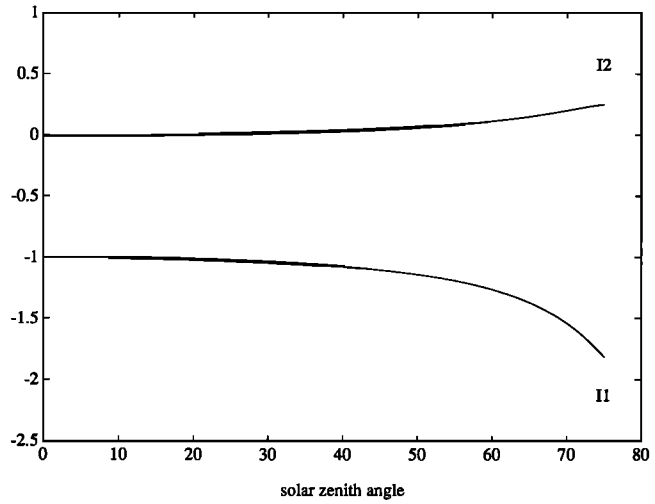

Fig. 4. Plots of I_1 and I_2 as a function of θ_s.

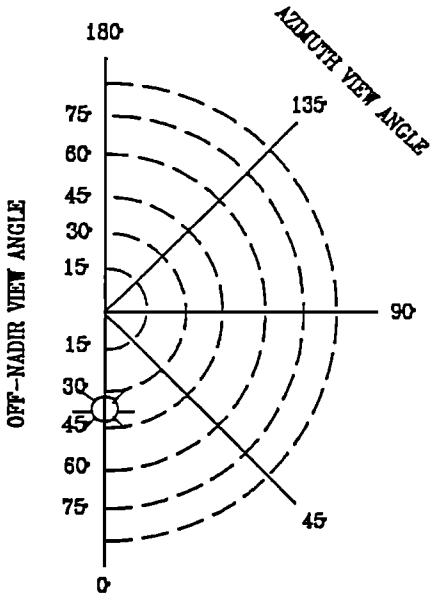

Fig. 5. Polar plot showing scheme for plotting bidirectional reflectance factors. The sun, indicated by sun symbol, is always located on the $\phi = 0°$ axis, the distance from the origin representing the sun zenith angle θ_s. The spectral bidirectional reflectance is defined in the polar plot, where the distance from the origin represents the off-nadir view angle θ_v, and the angle from $\phi = 0°$ represents the sensor's azimuth relative to the sun, ϕ. Curves in the polar plot appearing in Figures 6, 7, and 8 are isoreflectance curves.

I_1 and I_2 have been obtained by numerical fits with correlation coefficients equal to 0.9999 and 0.9993, respectively, in the range of θ_s between 0° and 75°. The function I_1 decreases while I_2 increases with θ_s, as can be seen in Figure 4.

Note that the volume component of our model does not account for the opposition effect phenomenon (also called hot spot) by which the probability of escape of a scattered photon in a volume of dispersed scatterers becomes close to 1 when the viewing direction approaches the sun direction, which results in an enhanced reflectance for this particular configuration. The opposition effect has been analyzed theoretically by a number of authors [*Hapke*, 1963, 1981, 1986; *Irvine*, 1966; *Lumme and Bowell*, 1981; *Verstraete et al.*, 1990] and has been shown to have an angular width which scales as $\pi/8\ (d/D)^3$, where d is the average size of a facet and D is the average distance between facets [*Hapke*, 1963, 1986]. Such a scaling suggests that the angular width of the hot spot is rather small, of the order of a few degrees, for current Earth canopies and bare grounds, which is confirmed by observations [*Gerstl*, 1988]. Since in remote sensing the sensor viewing configuration rarely coincides with the hot spot geometry, omitting this hot spot feature in the volume component of our model has limited consequences. Note besides that the geometric component ρ_{geom} (1) of our model has a local maximum in the hot spot geometry for sufficient sun elevation (section 2.2), since this particular geometry minimizes the amount of unviewed illuminated areas of the protrusion system with a total absence of apparent shadows.

3. Comparison With Observations

3.1. *Comparison Protocol*

The model has been tested against the in situ observations of *Kimes* [1983] and *Kimes et al.* [1985, 1986], which describe a wide variety of surface types and locations. *Kimes* [1983] has reported on measurements of bidirectional reflectance over different test sites, plowed field, corn field, orchard grass and grass lawn, near Beltsville, Maryland. In situ experiments were also made in northern Africa on various surface types, which have been labeled annual grassland, hard wheat, steppe, irrigated wheat, and soybean [*Kimes et al.*, 1985]. Helicopter measurements have been performed on two types of forest (pine and deciduous) in Virginia [*Kimes et al.*, 1986]. The range of LAI covered by these observations is rather wide, from zero (plowed field) to about 10 (grass lawn). We estimate that this data collection is fairly representative of most surface types of interest for applications of multitemporal remotely sensed data sets.

The above measurements were made on ground in the NOAA 7 AVHRR visible band (0.58–0.68 μm) and near-infrared band (0.73–1.1 μm) spectral bands using a Mark III radiometer with a field of view limited to 12°. For each measurement period, characterized by a given sun zenith angle θ_s, 41 directions were observed, located at nadir and at 15° increments of off-nadir viewing angle θ_v up to 75°, and 45° increments of azimuth angle ϕ (Figure 5).

Three different sun angles have been retained for each surface type. Thus the total number N of collected reflectance measurements per surface type is $N = 123$. The three parameters k_0, k_1, k_2 of our model have been derived for a given surface type by a least squares fit between model and observations, in order to minimize the residue δ, defined by

$$\delta^2 = \frac{1}{N} \sum_{i=1}^{N} [\rho_i - (\rho_{\text{obs}})_i]^2, \tag{16}$$

where ρ_i and $(\rho_{\text{obs}})_i$ refer to the modeled and observed reflectances for a given set of geometric angles (θ_s, θ_v, ϕ), respectively. Note that in this procedure, equal weight has been assigned for each observed reflectance and that the modeled ρ_i have by construction an azimuthal symmetry about the principal plane of the sun (0°/180° azimuths). The results of the fit for the visible and near-infrared spectral bands and all investigated surface types appear in Table 1.

TABLE 1. Comparison of the Model With Observations in the Visible and Near-Infrared Bands of *Kimes* [1983] and *Kimes et al.* [1985, 1986]

	Cover, Percent	LAI	Sun Angles θ_s, deg	Visible Spectral Band						Near-Infrared Spectral Band					
				k_0	k_1	k_2	δ_{obs}	rms of Fit δ	R^2	k_0	k_1	k_2	δ_{obs}	rms of Fit δ	R^2
Plowed field†	0		45, 30, 26	24.3	7.3	64.2	6.1	1.8	0.91	28.8	8.5	74.8	7.2	2.5	0.88
Annual grass†	4	—	50, 30, 28	34.9	4.4	37.7	4.1	1.7	0.84	45.2	5.3	50.3	5.4	2.4	0.80
Hard wheat†	11	0.28	51, 32, 27	27.3	5.2	26.9	4.0	1.2	0.91	37.3	3.3	80.2	6.7	2.4	0.87
Steppe†	18	—	63, 35, 27	26.6	5.0	5.9	4.8	2.7	0.68	35.6	5.6	21.7	5.9	3.0	0.74
Corn*	25	0.65	68, 46, 23	8.4	0.6	0.1	1.5	1.4	0.14	27.2	0	28.5	5.5	3.8	0.53
Orchard grass*	50	1.	71, 58, 45	7.9	1.2	9.0	2.3	1.0	0.80	26.5	1.5	43.0	8.4	4.1	0.76
Irrigated wheat†	70	4.	59, 42, 26	5.2	0.5	27.3	3.0	1.2	0.84	42.1	0	121.0	13.5	5.4	0.84
Pineforest‡	75	—	59, 41, 23	3.7	0	13.3	1.9	1.4	0.50	28.2	1.7	24.3	6.8	6.3	0.15
Deciduous forest‡	79	—	63, 45, 25	3.0	0	8.7	1.4	1.0	0.52	40.0	4.0	29.5	8.0	6.6	0.32
Soybean*	90	4.6	63, 49, 28	3.2	0	8.4	1.3	0.9	0.57	52.8	1.0	46.0	6.7	3.8	0.68
Grass lawn*	97	9.9	70, 56, 42	4.8	0	10.2	1.9	1.0	0.70	36.3	0	56.4	10.8	6.2	0.67

The surface parameters k_0, k_1, and k_2 (see text) are expressed in percent of reflectance, as are the residues (rms of fit) δ and δ_{obs}. R^2 is dimensionless. The observations are ordered with increasing percent vegetation coverage.

*From *Kimes* [1983].

†From *Kimes et al.* [1985].

‡From *Kimes et al.* [1986].

This table contains, for each surface type, the observed estimates of percent vegetation coverage and LAI, the three selected sun zenith angles, and for each spectral band, the resulting surface parameters k_0, k_1, k_2, expressed in percent of reflectance. This table also contains the residues δ (16) and δ_{obs} expressed in percent of reflectance, where δ_{obs} measures the magnitude of the bidirectional effects in the measurement data,

$$\delta_{obs}^2 = \frac{1}{N}\sum_{i=1}^{N}(\rho_{obs})_i^2 - \left[\frac{1}{N}\sum_{i=1}^{N}(\rho_{obs})_i\right]^2, \quad (17)$$

and the determination coefficient R^2, defined as

$$R^2 = 1 - \frac{\delta^2}{\delta_{obs}^2}. \quad (18)$$

3.2. *Results*

Table 1 shows that the model agrees reasonably well with the observations, since among the 22 investigated cases (11 surface types with two spectral bands), 19 have a correlation coefficient R^2 which ranges from 0.51 to 0.91. The proportion is 15 out of 22 with $R^2 > 2/3$, and nine out of 22 with $R^2 > 0.80$. We may consider that, for the sensor data correction and normalization problem, these results are quite satisfactory with regard to other sources of noise which affect space sensor data (atmospheric corrections, for example) and which also affect the in situ observations (data contamination by sky radiation, for example). There is some tendency to have better results for small vegetation coverage (less than 20%) rather than for high vegetation coverage (larger than 75%).

The behavior of the model as compared to the observations is illustrated in Figures 6, 7, and 8 corresponding to the cases of a plowed field, absence of vegetation, and a hard wheat field, respectively, representing a low LAI situation, and an irrigated wheat field, representing a relative large LAI situation (Table 1). Figures 6–8 display the general shape and numerical values of the isoreflectance curves, the azimuthal and radial gradients, and the position of local extrema, if any, show good agreement between model and observations. Figure 6 (plowed field) shows a relatively strong asymmetry about the $\phi = 90°$ plan, with a strong enhancement in the backscattering region and a depletion in the forward-scattering region. The radial (zenith) gradients remain moderate in general. A local maximum appears in the backscattering direction for both bands, close to the point $\theta_v \approx \theta_s$, $\phi = 0°$, for small values of θ_s, as predicted by the model analysis (section 2.2). In contrast, in Figure 8 (irrigated wheat), the major feature appearing at all sun angles and spectral bands is a minimum reflectance near nadir viewing, in the forward-scattering region ($\theta_v \approx 15$–$30°$, $\phi = 180°$). The reflectance increases with θ_v for all azimuths ϕ, with steep radial gradients for large θ_v, especially when θ_s is large ($\approx 60°$). The azimuthal dependence of the reflectance is significantly less for the irrigated wheat than for the plowed field. The hard wheat bidirectional signature (Figure 7) is somewhat intermediate between the two extremes of Figures 6 and 8.

The determination coefficient R^2 is less than 0.50 for three cases out of 22, which are those of corn in the visible, and pine and deciduous forests in the near infrared. There are few bidirectional effects in the case of corn ($\delta_{obs} \approx 0.015$). A model inefficiency at low δ_{obs} is not perceived as a real drawback, since the model aims at reducing the high-level fluctuations related to bidirectional effects in sensor data, while low-level bidirectional effects add to the various sources of noise which affect the data and, consequently, cannot be reduced.

In contrast, the case of the forests in the near infrared is characterized by a high magnitude of bidirectional effects (δ_{obs} of the order of 6–8%) together with a weak correlation ($R^2 < 0.30$) between model and observations. In fact, the analysis shows that the correlation coefficient R^2 increases up to acceptable values, in the range 0.50–0.80, when the original data set made of data acquired with three solar zenith angles θ_s is subdivided into two data subsets, the first with the two θ_s larger than 40°, and the second with a unique $\theta_s \approx 25°$ (see Table 2). The surface parameters k_0, k_1, k_2

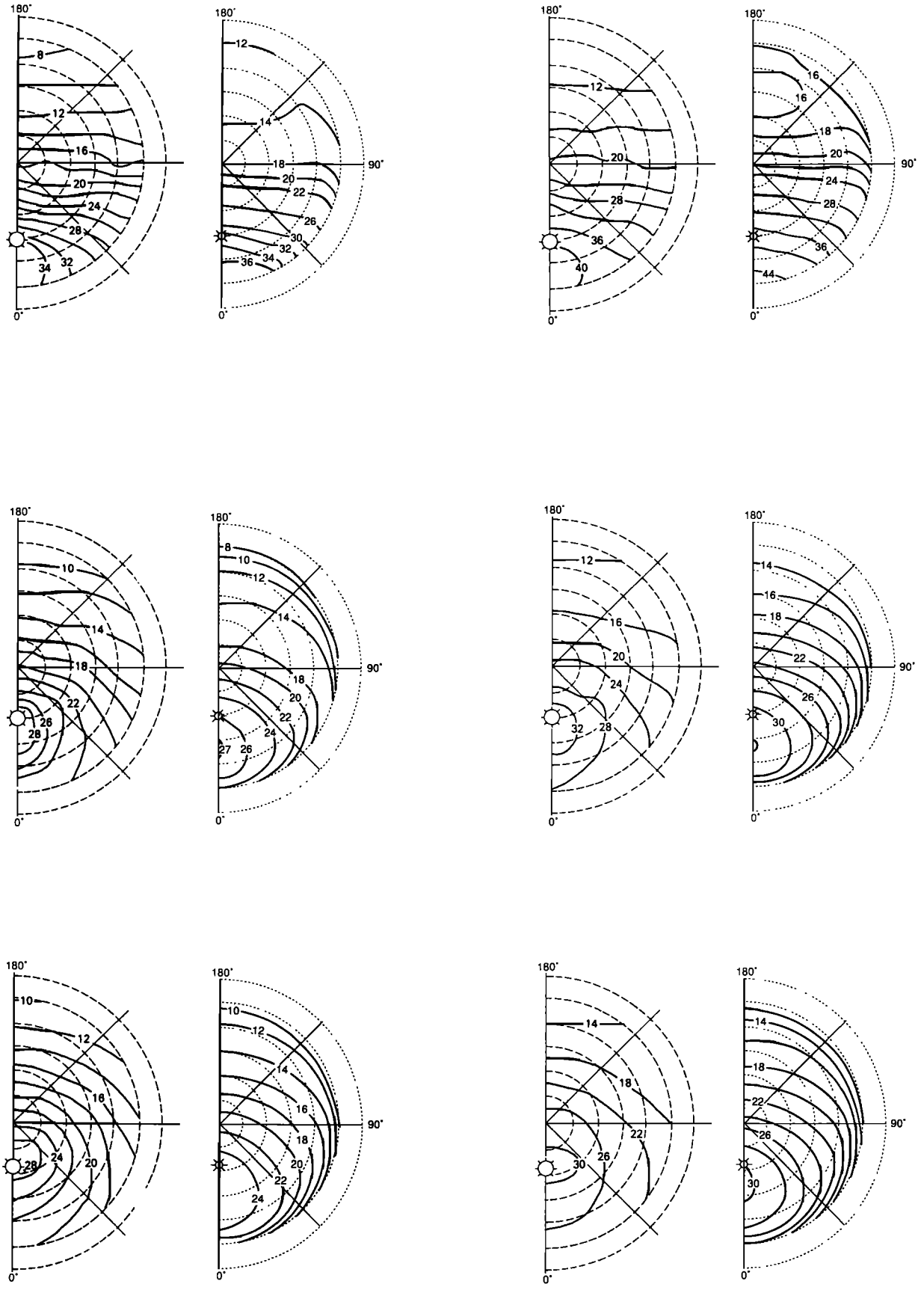

Fig. 6. Comparisons between the observations of (*a*) *Kimes et al.* [1985] and (*b*) our model for a plowed field in the visible (left) and near infrared (right) and three sun angles, θ_s = 45°, 30°, 26° (from top to bottom).

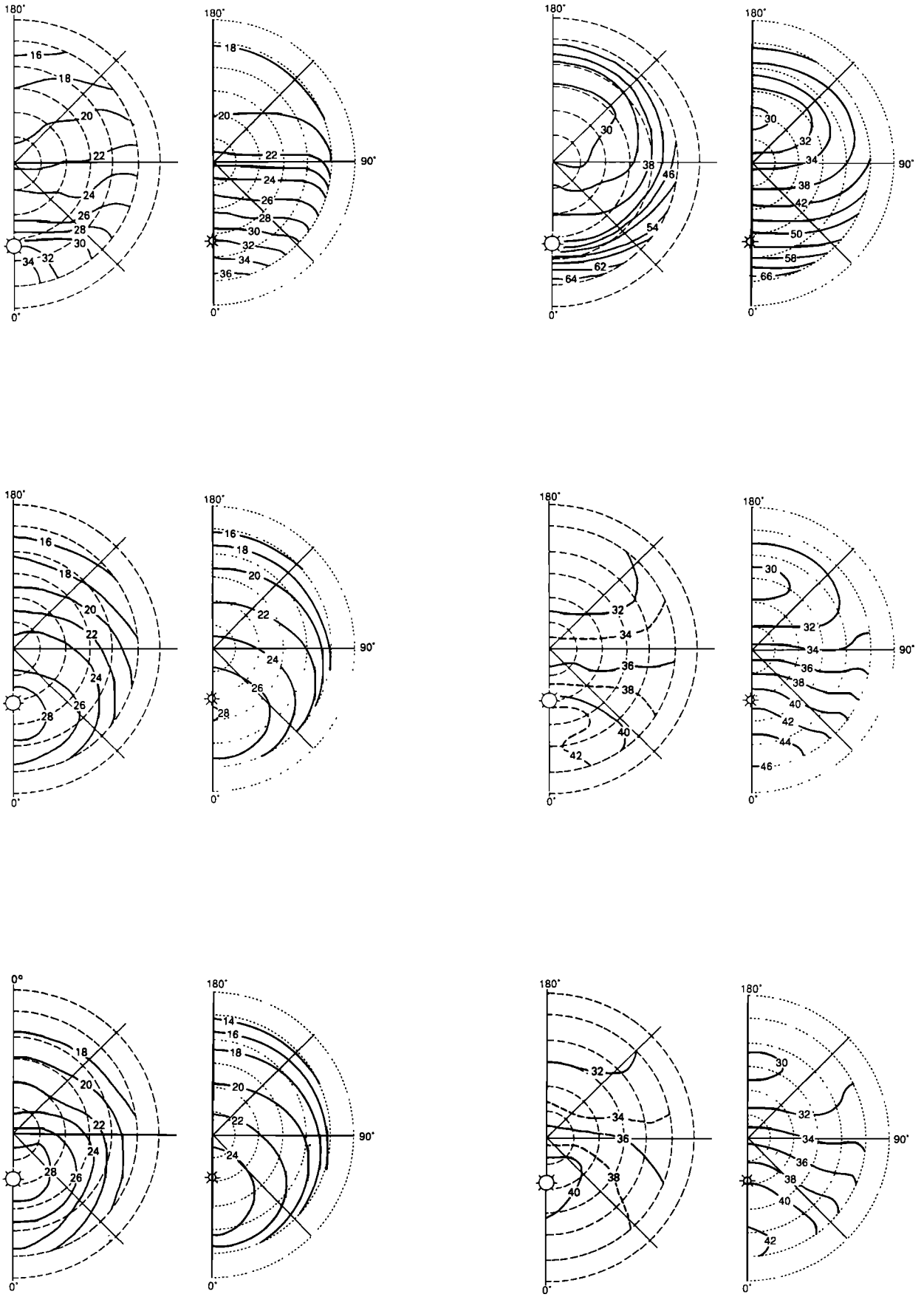

Fig. 7. Same as Figure 6 for hard wheat and θ_s = 51°, 32°, 27°.

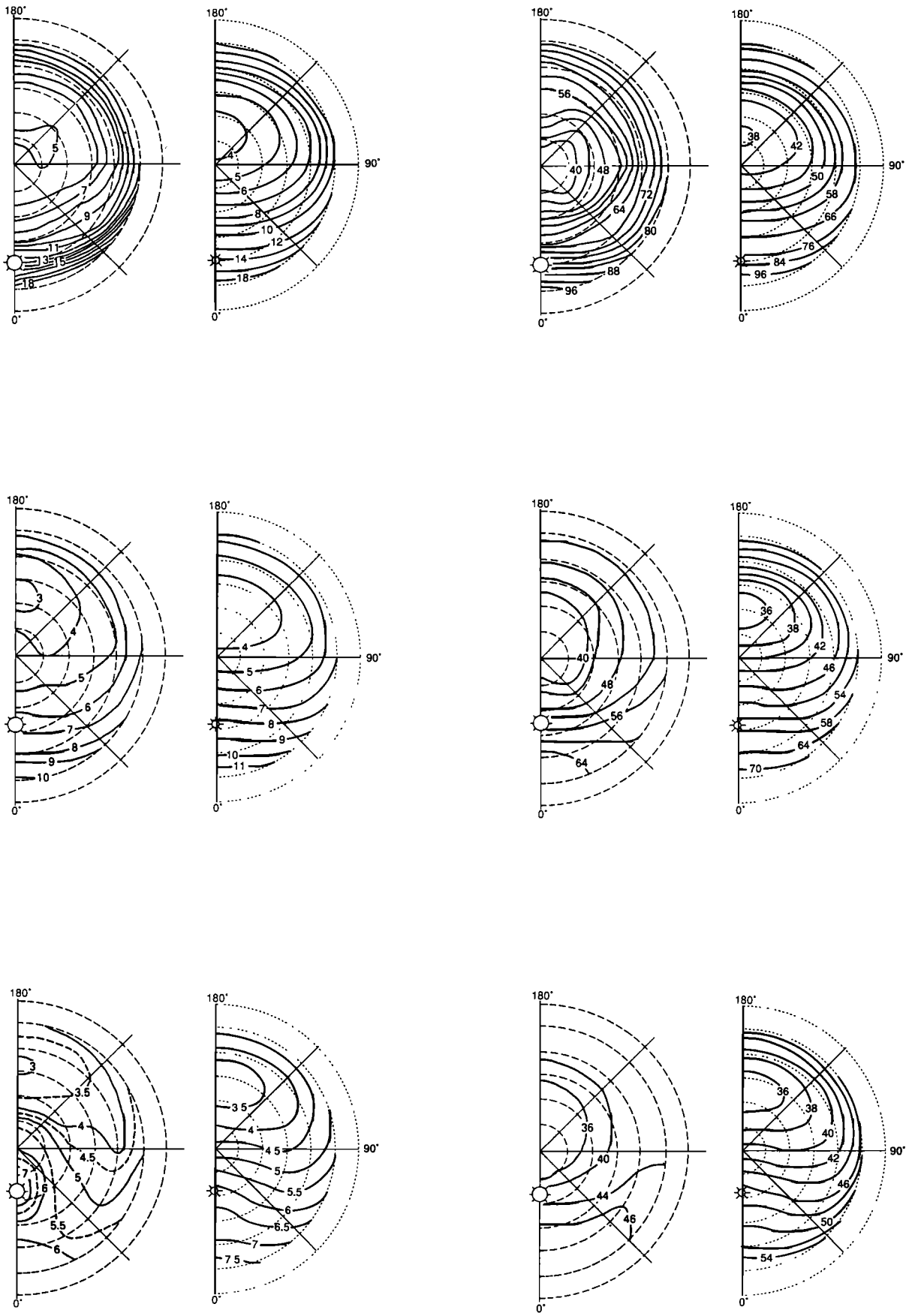

Fig. 8. Same as Figure 6 for irrigated wheat and θ_s = 59°, 42°, 26°.

TABLE 2. Comparison of the Model With Observations of *Kimes et al.* [1986] in the Visible and Near-Infrared Spectral Bands for Forest Cover Types and for Specific Sun Angle Values

Cover Type	Band	θ_s, deg	k_0	k_1	k_2	rms of fit δ	R^2
Pine forest	visible	59, 41	2.9	0	15.6	0.91	0.80
		23	4.9	0	34.0	0.82	0.71
	near infrared	59, 41	22.9	0.9	37.1	2.2	0.80
		23	36.1	3.4	133.0	4.1	0.57
Deciduous forest	visible	63, 45	2.6	0	9.8	0.91	0.67
		25	3.6	0	19.6	0.57	0.67
	near infrared	63, 45	34.8	3.7	43.2	3.74	0.76
		25	45.3	2.6	105.1	2.03	0.80

Units of parameters are the same as those in Table 1.

associated with the two subsets are then markedly different. This latter result suggests that as the radiation source moves toward the vertical direction, the contribution of the lower layers of the forest, more and more illuminated, becomes quite important and produces a significantly different bidirectional behavior than the upper layers formed by the trees. The application of our model to forest surfaces might therefore be questionable when used with a large range of sun angles.

As expected, the k_0 parameter, which represents the surface reflectance when both sun and sensor are at nadir, tends to decrease as LAI increases in the visible band, while no such tendency is seen in the near-infrared band. As also expected, the k_1 parameter, which determines the magnitude of geometric and shadowing effects, is significant only when LAI is weak (<0.5), and becomes negligible for larger LAI. The k_1 parameter has been set to zero in Table 1, as the numerical solution of the least squares fit sometimes provides slightly negative (and unphysical) k_1 values. When k_1 is nonnegligible (small LAI), the k_1 value leads to realistic values of the ratio hl/S, of the order of 0.1–0.5.

Interestingly, the ratio k_1/k_0, which roughly scales as hl/S at small LAI in our model, and thus should be independent of the spectral band, does satisfy this prediction, since k_1/k_0 has nearly the same value (to within 7%) in the two spectral bands of Table 1 for the plowed field and annual grassland cases (vegetation cover less than 4%).

The k_2 parameter takes rather high values in the two spectral bands for both small and large LAI cases. This suggests that volume effects on the reflectance are significant for all surface types, vegetated or not. It is obvious that volume effects should be dominant in dense vegetation canopies. The fact that these effects are also important in bare soils is clearly established in our data; we have thus verified, in the example of the plowed field, that R^2 goes from 0.91 and 0.88 to 0.46 and 0.44 for the visible and near-infrared spectral bands, respectively, when the k_2 parameter is artificially forced to be set to zero. The volume effects in bare soils are likely to be due to their porosity and to the presence of microdust [*Hapke*, 1963, 1981].

The values of k_2 can reach 0.27 (visible) and 1.21 (near infrared) for the irrigated wheat, and 0.64 (visible) and 0.75 (near infrared) for the plowed field (Table 1). These values are higher than expected, since according to our model, the k_2 parameter primarily stands for a facet reflectance (13), with typical expected values of 0.1 and 0.5 for leaves in the visible and near-infrared spectral bands, and of 0.2–0.4 for soil facets. These discrepancies are due to the various assumptions made in our model, the most critical assumption being presumably to have considered an isotropic facet distribution function; we observe that the larger values of k_2 obtained in vegetated surfaces are those of hard wheat and irrigated wheat, which are highly erectophile. Note, however, that the ratio of k_2 in the two bands has a typical value for vegetated surfaces of about 3–5, in agreement with the expected ratio of leaf reflectances in the near-infrared and visible spectral bands.

4. DISCUSSION

We briefly comment on the consequences of these results for the reduction of bidirectional effects in space observations. In this study, our model has been tested against a complete data set of unitemporal in situ observations, where the retrieved parameters k_0, k_1, and k_2 characterize the surface properties at a given date. Applications of this model to space observations such as those of AVHRR/NOAA define a more complicated task, since one terrestrial target is viewed at most once a day with different viewing angles. Even after having performed atmospheric corrections, a bidirectional model is needed to reduce the variabilities (and thus errors) [*Roujean et al.*, 1992]. The model parameters must be derived from the observed time series, using regression techniques between the observed and modeled reflectances. This regression should be made in subperiods chosen short enough to consider the surface as time invariant, and long enough to contain a number of sensor data sufficient to apply the regression (at least four). A possibility to normalize satellite data is then to replace the original time series of observed reflectances by a time series of the k_0 parameter obtained on each subperiod of the period of observation. Since k_0 represents physically the target reflectance observed at nadir with a sun at zenith, k_0 may be called a normalized reflectance and provides a basis for the intercomparison of sensor data acquired with different viewing or sun angles. Preliminary results using this method, obtained with an atmospherically corrected AVHRR data set during a vegetation annual cycle over three vegetated and semi-arid test sites in France, have been found to be quite encouraging [*Roujean and Leroy*, 1991]. A more detailed experimental analysis, covering a wider variety of test sites, will be the subject of a forthcoming publication.

5. CONCLUSION

A new model of the surface bidirectional reflectance for the correction and normalization of remotely sensed multi-

temporal data sets has been presented in this paper. The model basically follows a semiempirical approach. On the one hand, the model has been constructed with only three surface parameters for reasons of practicality of correction algorithms, a number perceived as very small to address the complexity of real situations at the length scale of a sensor pixel, but sufficient to take into account the major physical trends. On the other hand, simple physical representations of idealized situations (opaque vertical protrusions oriented at random and associated shadowing effects, single scattering homogeneous volumes of dispersed facets to represent volume scattering in canopies and dust of bare soils) have been used as a guide to obtain the functional dependence of the surface reflectance upon the three variables θ_s, θ_v, and ϕ. This phenomenological approach is thus significantly different from the strictly empirical approach followed by *Minnaert* [1941], *Walthall et al.* [1985], and *Shibayama and Wiegand* [1985] for a problem similar to that treated here and, by contrast, has some resemblance to the three-parameter water cloud model of *Attema and Ulaby* [1978] applicable in the microwave domain.

The resulting analytical model (10) is numerically tractable, and its linearity in terms of surface parameters makes it applicable to heterogeneous surfaces, a situation most common when considering the surfaces covered by remote sensing pixels. Detailed comparisons between the model and in situ observations over a wide variety of surfaces with various degrees of vegetation cover show satisfactory agreement with correlation coefficients R^2 ranging between 0.50 and 0.91 for most investigated surface types in the visible and near-infrared spectral bands. The model appears therefore as a good candidate for substantially reducing the undesirable large-amplitude fluctuations related to surface bidirectional effects in remotely sensed multitemporal data sets. However, although our three surface parameters are analytically related to more basic model parameters (roughness, facets reflectance, facet area index, etc.), which proves useful in the understanding of the observational data reduction process (see section 3), it is still not possible at this point, considering the series of assumptions made in the model derivation, to assure that an inverse interpretation of these three surface parameters in terms of observed physical properties of the surface is indeed feasible.

APPENDIX

We derive in this appendix the geometric scattering component ρ_{geom} (equations (1) and (2)) of our model. This component is evaluated by assuming that the subpixel surface contains a large number of identical protrusions with rectangular, vertical wall shape, disposed on a horizontal surface (Figure 1).

Each protrusion is thus made of a vertical wall of height h, width b, and length l much larger than b and h (Figure A1). Let n be the total number of protrusions on the subpixel surface and S the average horizontal surface per protrusion. The total horizontal surface of the subpixel surface is thus nS. The space between protrusions is assumed such that mutual shadowing between protrusions can be neglected, that is to say, we consider ranges of parameters such that $hltg\theta_s \leq S$ and $hltg\theta_v \leq S$.

We assume that each illuminated surface of the system "protrusions + reference surface" is Lambertian with reflectance ρ_0 and that the shadowed areas are absolutely dark.

Let $\mathbf{s}$ and $\mathbf{v}$ be unit vectors along the sun and viewing directions, respectively. Let the orientation of each protrusion i, $i = 1$–n, be characterized by a unit vector $\mathbf{n}_i$ normal to its illuminated long vertical side ($\mathbf{n}_i \cdot \mathbf{s} \leq 0$ with the sign conventions of Figure A1). The position of $\mathbf{n}_i$ in the horizontal plane is described by the azimuth $(\phi_n)_i$. Let $(s_h)_i$ be, for a given sun-surface-sensor configuration, the total horizontal surface associated with protrusion i which cannot contribute to the reflected power budget, because this surface is either not illuminated or not viewed. Finally, let $(s_v)_i$ be the surface of the long vertical wall of protrusion i, provided that this surface is illuminated and viewed ($(s_v)_i = 0$ otherwise). The power δW reflected along $\mathbf{v}$ in the elementary solid angle $d\Omega_v$, originating from the system of Figure A1, may be written as

$$\delta W = \left(nS - \sum_{i=1}^{n} (s_h)_i \right) L_h \cos\theta_v \, d\Omega_v + \sum_{i=1}^{n} (s_v)_i |\mathbf{n}_i \cdot \mathbf{v}| (L_v)_i \, d\Omega_v \qquad \text{(A1)}$$

In (A1), L_h is the radiance reflected by the horizontal surfaces and $(L_v)_i$ is the radiance reflected by the vertical wall of protrusion i. These radiances read

$$L_h = \frac{1}{\pi} \rho_0 E_s \cos\theta_s \qquad \text{(A2)}$$

$$(L_v)_i = \frac{1}{\pi} \rho_0 E_s |\mathbf{n}_i \cdot \mathbf{s}| \qquad \text{(A3)}$$

where E_s is the solar irradiance.

The global reflectance ρ_{geom} of the subpixel surface is related to δW by

$$\rho_{\text{geom}} = \frac{\pi \delta W}{nS \cos\theta_v \cos\theta_s E_s \, d\Omega_v} \qquad \text{(A4)}$$

which, after combination with (A1)–(A3), gives

$$\rho_{\text{geom}} = \rho_0 \left\{ \left[1 - \left(\sum_{i=1}^{n} (s_h)_i / nS \right) \right] + \left[\left(\sum_{i=1}^{n} (s_v)_i |\mathbf{n}_i \cdot \mathbf{s}| \, |\mathbf{n}_i \cdot \mathbf{v}| \right) \Big/ (nS \cos\theta_s \cos\theta_v) \right] \right\} \qquad \text{(A5)}$$

The discrete sums appearing in (A5) are in fact averages of quantities which depend only upon the orientation of the protrusions. Since n is a large number and the protrusion orientations are assumed to be at random, the discrete sums in (A5) may be approximated by continuous integrals. The expression of ρ_{geom} may then be rewritten as

$$\rho_{\text{geom}} = \rho_0 \left[\left(1 - \frac{1}{\pi S} \int_{\phi_s - (\pi/2)}^{\phi_s + (\pi/2)} s_h(\phi_n) \, d\phi_n \right) \right.$$

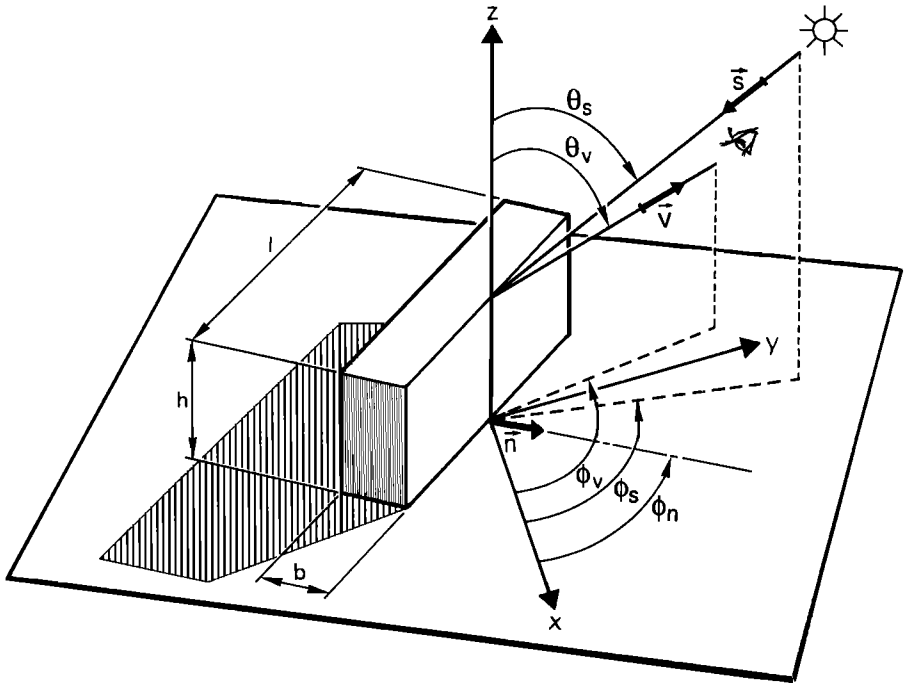

Fig. A1. A long-wall protrusion and associated shadows. Note that $\phi = |\phi_v - \phi_s|$.

$$+\frac{1}{\cos\theta_s \cos\theta_v \pi S}\int_{\phi_s-(\pi/2)}^{\phi_s+(\pi/2)} s_v(\phi_n)\,|\mathbf{n}\cdot\mathbf{s}|\,|\mathbf{n}\cdot\mathbf{v}|\,d\phi_n\Bigg] \tag{A6}$$

in which the integration variable is the protrusion orientation azimuth ϕ_n and the integration domain covers all possible protrusion orientations, that is, $\phi_n \in [\phi_s - (\pi/2), \phi_s + (\pi/2)]$.

Parameters $s_h(\phi_n)$ and $s_v(\phi_n)$ remain to be estimated. Note that we have neglected in (A1), (A5), and (A6) the contributions of the two vertical ends of the walls to the illuminated and viewed surfaces. The derivation of $s_h(\phi_n)$ below also assumes that the contributions of the two protrusion ends to the budget of unviewed or shadowed horizontal surfaces can be neglected. These assumptions are justified to order b/l except when the sun direction is nearly aligned with the main direction of the wall. The range of wall azimuth ϕ_n for which this latter condition is satisfied scales also as b/l and can be neglected in the integrals of (A6) leading to ρ_{geom}.

It is necessary, for the evaluation of $s_h(\phi_n)$ and $s_v(\phi_n)$, to distinguish three different cases according to the respective configurations of the wall normal $\mathbf{n}$ and of the sun and viewing directions.

1. The sensor is on the shadowed side of the wall, that is,

$$|\phi_v - \phi_n| \geq \frac{\pi}{2} \geq |\phi_s - \phi_n|, \tag{A7}$$

In this case,

$$s_h(\phi_n) = htg\theta_s \cos(\phi_s - \phi_n) - htg\theta_v \cos(\phi_v - \phi_n)$$
$$s_v(\phi_n) = 0. \tag{A8}$$

Note that $htg\theta_s \cos(\phi_s - \phi_n)$ and $htg\theta_v \cos(\phi_v - \phi_n)$ are the width of the horizontal shadowed area and the width of the horizontal unviewed area along the wall, respectively.

2. The sensor is on the illuminated side of the wall but sufficiently inclined so that most of the horizontal shadowed area is not viewed, i.e.,

$$tg\theta_v \cos(\phi_v - \phi_n) \geq tg\theta_s \cos(\phi_s - \phi_n) \geq 0. \tag{A9}$$

Then

$$s_h(\phi_n) = hltg\theta_v \cos(\phi_v - \phi_n)$$
$$s_v(\phi_n) = hl. \tag{A10}$$

We have neglected in the derivation of $s_h(\phi_n)$ in (A10) the terms scaling as h^2 which result from the fact that when $\phi_v \neq \phi_s$, there is always some shadow viewed by the sensor in the vicinity of the ends of the wall.

3. The sensor is on the illuminated side of the wall, and the view direction is sufficiently high that the following condition holds:

$$tg\theta_s \cos(\phi_s - \phi_n) \geq tg\theta_v \cos(\phi_v - \phi_n) \geq 0 \tag{A11}$$

Then in this case, neglecting as above the terms in h^2,

$$s_h(\phi_n) = hltg\theta_s \cos(\phi_s - \phi_n)$$
$$s_v(\phi_n) = hl. \tag{A12}$$

In (A6), the angular domain of ϕ_n may be subdivided into three distinct domains, $[-(\pi/2) + \phi_s, \phi_v - (\pi/2)]$, $[\phi_v - (\pi/2), \phi_0]$, $[\phi_0, \phi_s + (\pi/2)]$, corresponding to the expressions (A8), (A12), and (A10), respectively, of $s_h(\phi_n)$ and $s_v(\phi_n)$, where ϕ_0 is an angle between $(\phi_s - (\pi/2))$ and $(\phi_s + (\pi/2))$ defined by

$$tg\theta_s \cos(\phi_s - \phi_0) = tg\theta_v \cos(\phi_v - \phi_0) \quad \text{(A13)}$$

and where $0 \leq (\phi_v - \phi_s) \leq \pi$ has been assumed by convention.

The expressions (1), (2) of the text for ρ_{geom} result from the calculation of the integral in (A6), where (A8), (A12), and (A10) of $s_h(\phi_n)$ and $s_v(\phi_n)$ have been applied.

Acknowledgments. The authors are indebted to A. Podaire (LERTS) for many useful discussions and suggestions throughout this work. We also thank D. S. Kimes (NASA/GSFC) for kindly providing the in situ data in digital form, and B. Pinty and Y. Kerr (both from LERTS) for a critical reading of the manuscript. Finally, we thank an unknown reviewer for many useful comments on the manuscript. One of us (J.L.R.) received doctoral financial support from Ministère de la Recherche et de la Technologie, and Centre National d'Etudes Spatiales.

REFERENCES

Attema, E.P.W., and F. T. Ulaby, Vegetation model as a water cloud, *Radio Sci.*, *13*(2), 357–364, 1978.

Camillo, P., A canopy reflectance model based on a analytical solution to the multiple scattering equation, *Remote Sens. Environ.*, *23*, 453–477, 1987.

Coulson, K. L., Effects of reflection properties of natural surfaces in aerial reconnaissance, *Appl. Opt.*, *5*(6), 905–917, 1966.

Coulson, K. L., and D. W. Reynolds, The spectral reflectance of natural surfaces, *J. Appl. Meteorol.*, *10*, 1285–1295, 1971.

Deering, D. W., and T. F. Eck, Atmospheric optical depth effects on angular anisotropy of plant canopy reflectance, *Int. J. Remote Sens.*, *8*(6), 893–916, 1987.

Deering, D. W., and P. Leone, A sphere-scanning radiometer for rapid directional measurements of sky and ground radiance, *Int. J. Remote Sens.*, *19*, 1–24, 1986.

Deering, D. W., T. F. Eck, and J. Otterman, Bidirectional reflectances of selected desert surfaces and their three-parameter soil characterization, *Agric. Forest Meteorol.*, *52*, 71–93, 1990.

Eaton, F. D., and I. Dirmhirn, Reflected irradiances indicatrices of natural surfaces and their effect on albedo, *Appl. Opt.*, *18*(7), 994–1008, 1979.

Egbert, D. D., Determination of the optical bidirectional reflectance from shadowing parameters, Ph.D. dissertation, University of Kansas, Lawrence, March 1976. (Available from University Microfilms, University of Michigan, Ann Arbor.)

Egbert, D. D., A practical method for correcting bidirectional reflectance variations, Proceedings of the Machine Processing of Remotely Sensed Data Symposium, pp. 178–189, 1977.

Gerstl, S.A.W., The angular reflectance signature of the canopy hotspot in the optical regime, Proceedings of the 4th International Colloquium on Spectral Signatures of Objects in Remote Sensing, *Rep. ESA SP-287*, Eur. Space Agency, Paris, France, April 1988.

Goel, N. S., Models of vegetation canopy reflectance and their use in estimation of biophysical parameters from reflectance data, *Remote Sens. Rev.*, *4*, 1–212, 1988.

Gutman, G., The derivation of vegetation indices from AVHRR data, *Int. J. Remote Sens.*, *8*, 1235–1243, 1987.

Hapke, B., A theoretical photometric function for the lunar surface, *J. Geophys. Res.*, *68*(15), 4571–4586, 1963.

Hapke, B., Bidirectional reflectance spectroscopy, 1, Theory, *J. Geophys. Res.*, *86*(B4), 3039–3054, 1981.

Hapke, B., Bidirectional reflectance spectroscopy, 4, The extinction coefficient and the opposition effect, *Icarus*, *67*, 264–280, 1986.

Hapke, B., and H. van Horn, Photometric studies of complex surfaces, with applications to the moon, *J. Geophys. Res.*, *68*(15), 4545–4570, 1963.

Irvine, W. M., The shadowing effect in diffuse radiation, *J. Geophys. Res.*, *71*(12), 2931–2937, 1966.

Kimes, D. S., Dynamics of directional reflectance factor distribution for vegetation canopies, *Appl. Opt.*, *22*(9), 1364–1372, 1983.

Kimes, D. S., W. W. Newcomb, C. J. Tucker, I. S. Zonneveld, W. van Wijngaarden, J. de Leeuw, and G. F. Epema, Directional reflectance factor distributions for cover types of Northern Africa, *Remote Sens. Environ.*, *18*, 1–19, 1985.

Kimes, D. S., W. W. Newcomb, R. F. Nelson, and J. B. Schutt, Directional reflectance distributions of a hardwood and a pine forest canopy, *IEEE Trans. Geosci. Remote Sens.*, *GE-24*(2), 281–293, 1986.

Kriebel, K. T., Measured spectral bidirectional reflection properties of four vegetated surfaces, *Appl. Opt.*, *17*(2), 253–259, 1978.

Lumme, K., and E. Bowell, Radiative transfer in the surfaces of atmosphereless bodies, *Astron. J.*, *86*(11), 1694–1704, 1981.

Minnaert, M., The reciprocity principle in lunar photometry, *Astrophys. J.*, *93*, 403–410, 1941.

Norman, J. M., J. M. Welles, and E. A. Walter, Contrasts among bidirectional reflectance of leaves, canopies, and soils, *IEEE Trans. Geosci. Remote Sens.*, *GE-23*(5), 659–667, 1985.

Otterman, J., Plane with protrusions as an atmospheric boundary, *J. Geophys. Res.*, *86*(C7), 6627–6630, 1981.

Otterman, J., and G. H. Weiss, Reflection from a field of randomly located vertical protrusions, *Appl. Opt.*, *23*(12), 1931–1936, 1984.

Rondeaux, G., Polarisation de la lumière réfléchie par un couvert végétal, Thèse de Doctorat de l'Université Paris VII, spécialité Méthodes Physiques en Télédétection, June 1990.

Ross, J. K., *The Radiation Regime and Architecture of Plant Stands*, W. Junk, The Hague, Netherlands, 1981.

Roujean, J. L., and M. Leroy, Normalisation des effets bidirectionnels de la réflectance de surface sur une série de données multitemporelles NOAA/AVHRR, Proceedings of the Fifth International Colloquium, Physical Measurements and Signatures in Remote Sensing, Courchevel, Jan. 14–18, 1991. (Available from ESA Publ. Div., Eur. Space Res. and Technol. Cent., Noorwijk, Netherlands.)

Roujean, J. L., M. Leroy, P. Y. Deschamps, and A. Podaire, Evidence of surface reflectance bidirectional effects from a NOAA/AVHRR multitemporal data set, *Int. J. Remote Sens.*, *13*, 685–698, 1992.

Shibayama, M., and C. L. Wiegand, View azimuth and zenith, and solar angle effects on wheat canopy reflectance, *Remote Sens. Environ.*, *18*, 91–103, 1985.

Suits, G. H., The calculation of the directional reflectance of a vegetative canopy, *Remote Sens. Environ.*, *2*, 117–125, 1972.

Taylor, V. R., and L. L. Stowe, Reflectance characteristics of uniform Earth and cloud surfaces derived from Nimbus 7 ERB, *J. Geophys. Res.*, *89*(D4), 4987–4996, 1984.

Verhoef, W., Light scattering by leaf layers with application to canopy reflectance modeling: The SAIL model, *Remote Sens. Environ.*, *16*, 125–141, 1984.

Verhoef, W., Earth observation modeling based on layer scattering matrices, *Remote Sens. Environ.*, *17*, 165–178, 1985.

Verstraete, M. M., B. Pinty, and R. E. Dickinson, A physical model of the bidirectional reflectance of vegetation canopies, 1, Theory, *J. Geophys. Res.*, *95*(D8), 11,755–11,765, 1990.

Walthall, C. L., J. M. Norman, J. M. Welles, G. Campbell, and B. L. Blad, Simple equation to approximate the bidirectional reflectance from vegetative canopies and bare soil surfaces, *Appl. Opt.*, *24*(3), 383–387, 1985.

P.-Y. Deschamps, Laboratoire d'Optique Atmosphérique, Université des Sciences et Techniques de Lille, 59655 Villeneuve d'Asq, France.

M. Leroy, Centre National d'Etudes Spatiales, 18 Avenue Edouard Belin, 31055 Toulouse Cedex, France.

J.-L. Roujean, Centre National de Recherches Météorologiques, 42 Avenue Gustave Coriolis, 31057 Toulouse, France.

(Received February 19, 1991;
revised June 4, 1992;
accepted June 5, 1992.)